PCCP

Accepted Manuscript

ROYAL SOCIETY OF CHEMISTRY

www.rsc.org/pccp

Physical Chemistry Chemical Physics
CREATED USING THE RSC LaTeX PCCP ARTICLE TEMPLATE – SEE www.rsc.org/electronicfiles FOR DETAILS
ARTICLE TYPE www. rsc.org/xxxxxx | XXXXXXXX

Enhanced thermoelectric performance in the *p*-type Half-Heusler (Ti/Zr/Hf)$CoSb_{0.8}Sn_{0.2}$ system via phase separation

Elisabeth Rausch,[a,b] Benjamin Balke,*[a] Siham Ouardi,[b] and Claudia Felser[b]

Received Xth XXXXXXXXXX 20XX, Accepted Xth XXXXXXXXX 20XX
First published on the web Xth XXXXXXXXXX 200X
DOI: 10.1039/b000000x

A novel approach for optimization of the thermoelectric properties of *p*-type Heusler compounds with a $C1_b$ structure was investigated. A successful recipe for achieving intrinsic phase separation in the *n*-type material based on the TiNiSn system is isoelectronic partial substitution of Ti with its heavier homologues Zr and Hf. We applied this concept to the *p*-type system *M*$CoSb_{0.8}Sn_{0.2}$ by a systematic investigation of samples with different compositions at the Ti position (*M* = Ti, Zr, Hf, $Ti_{0.5}Zr_{0.5}$, $Zr_{0.5}Hf_{0.5}$, and $Ti_{0.5}Hf_{0.5}$). We thus achieved an approximately 40% reduction of the thermal conductivity and a maximum figure of merit *ZT* of 0.9 at 700 °C. This is a 80% improvement in peak *ZT* from 0.5 to 0.9 at 700 °C compared to the best published value of an ingot *p*-type Half-Heusler compound. Thus far, comparable good thermoelectric *p*-type materials of this structure type have only been realized by a nanostructuring process via ball milling of premelted ingot samples followed by a rapid consolidation method, like hot pressing. The herein-presented simple arc-melting fabrication method reduces the fabrication time as compared to this multi-step nanostructuring process. The high mechanical stability of the Heusler compounds is favorable for the construction of thermoelectric modules. The Vickers hardness values are close to those of the *n*-type material, leading to good co-processability of both materials.

1 Introduction

Thermoelectric (TE) materials directly transform waste heat into useful electricity. TE devices are composed of pairs of *n*-type and *p*-type materials. The efficiency of a TE material is characterized by its dimensionless figure of merit $ZT = S^2\sigma T/\kappa$, where *S* is the Seebeck coefficient (also known as the thermopower), σ the electrical conductivity, κ the total thermal conductivity, and *T* the absolute working temperature. Unfortunately, all these physical properties are interdependent and cannot be manipulated separately. Different TE materials are used depending on the operating temperatures. At moderate temperatures, such as in industrial waste heat and automobiles (*T* = 500-800 °C), several materials such as PbTe alloys[1] and SiGe[2] are used. Among the various material, Heusler compounds have recently gained attention as promising materials for TE applications.[3–7] The advantage of Heusler compounds are excellent electronic properties[8,9] and high thermal and mechanical stability.[6] These compounds are made of earth-abundant elements and they are environmentally friendly,[10] which are important issues from the economical point of view.

Heusler compounds for TE applications are intermetallic compounds crystallizing in a $C1_b$ structure with the formula *M*NiSn for the *n*-type and *M*CoSb for the *p*-type. *M* is either Ti, Zr, or Hf or a combination of these elements. Currently, 20% substitution of Sb by Sn in *M*CoSb has achieved the best *p*-type Heusler compound.[4,5,7,11,12] However, the relatively high thermal conductivity is an obstacle to implementing Heusler TE's. The total thermal conductivity consists of an electronic and a lattice contribution. In general, the phonon contribution can be reduced effectively by point and mass defect scattering by forming a solid solution or by additional boundary scattering through a reduction of the grain size or phase separation. Several studies have succeeded in reducing the lattice thermal conductivity of Heusler compounds by embedding nanoparticles such as HfO_2 inclusions.[12] The most successful improvement of the TE properties of state-of-the-art *p*-type materials involves the artificial reduction of the grain size via ball milling.[5,11] The authors claim that the *ZT* improvement of 60% from 0.5 to 0.8 in $Zr_{0.5}Hf_{0.5}CoSb_{0.8}Sn_{0.2}$ comes from a simultaneous increase in the Seebeck coefficient and a significant decrease in thermal conductivity due to the nanostructuring. The benchmark of *ZT* = 1.0 in $Hf_{0.8}Ti_{0.2}CoSb_{0.8}Sn_{0.2}$ was reached by replacing Zr with its heavier homologue Hf by a similar fabrication process.[5] Another concept to achieve high thermoelectric performance in bulk materials is phase separation on a micro- or nano-meter scale. Investigations have mainly focused on the PbTe, PbSe, and PbS systems.[13] For example, the precipita-

[a] *Institut für Anorganische und Analytische Chemie, Johannes Gutenberg-Universität, 55099 Mainz, Germany; * E-mail: balke@uni-mainz.de*
[b] *Max Planck Institute for Chemical Physics of Solids, 01187 Dresden, Germany.*

tion of a second phase in PbTe + 12% PbS led to a reduction of approximately 50% of the lattice thermal conductivity to 0.45 W $m^{-1}K$.[14] Recently, *ZT* values up to 2 were reported for *p*-type $Ge_{0.87}Pb_{0.13}Te$ as a result of sub-micron phase separation.[15]

The thermoelectric performance of Heusler materials can also be improved by phase separation.[16–19] Recently, the outstanding thermoelectric properties of a *n*-type material with *ZT* up to 1.4 based on doped $Ti_{0.5}Zr_{0.25}Hf_{0.25}NiSn$[20,21] were explained by Schwall and Balke.[22] The samples exhibited a microstructure composed of three coexisting $C1_b$ phases that were rich in either Ti or Hf.

This work investigates how intrinsic phase separation can be generated in the *p*-type system $MCoSb_{0.8}Sn_{0.2}$ by isoelectronic substitution on the *M*-position and its effect on the thermoelectric properties. Our investigation on the thermoelectric properties of this system proves a 40% reduction of the thermal conductivity due to the phase separation in $Ti_{0.5}Hf_{0.5}CoSb_{0.8}Sn_{0.2}$ compared to the single phase $TiCoSb_{0.8}Sn_{0.2}$ leading to a maximum figure of merit *ZT* of 0.9 at 700 °C. Compared to the best published value of an ingot *p*-type Half-Heusler compound by Yan et al.[4] with the composition $Zr_{0.5}Hf_{0.5}CoSb_{0.8}Sn_{0.2}$ this is an 80% improvement in peak *ZT* from 0.5 to 0.9 at 700 °C. Due to importance of the mechanical stability of the materials for the fabrication of TE modules, we investigated the Vickers hardness of the materials as well.

2 Experimental details

Ingots of (Ti/Zr/Hf)$CoSb_{0.8}Sn_{0.2}$ were prepared by arc melting stoichiometric amounts of the elements in an Ar atmosphere. For homogenization, each sample was flipped and remelted several times. The weight loss due to the high vapor pressure of Sb was compensated for by crushing the sample and adding the appropriate amount of Sb. This step was repeated twice. Subsequently, the ingots were annealed under vacuum in quartz ampules at 900 °C for 7 days, followed by quenching in ice water.

The crystal structure was verified by powder X-ray diffraction (PXRD) on a Seifert XRD 3000TT using Cu Kα radiation (λ = 1.5418 Å) in Bragg-Brentano geometry with an automatic divergence slit. The microstructure of the polished samples was investigated by scanning electron microscopy (SEM, FEI Nova NanoSEM 630) and the composition was analyzed by energy-dispersive X-ray (EDX) spectroscopy. A standardless ZAF correction was applied for quantitative evaluation by means of the EDAX software. The samples were cut into bars and polished for the simultaneous measurement of conductivity and Seebeck coefficients by a LSR-3 (Linseis) in a He atmosphere. The thermal conductivity was calculated from diffusivity measurements by a Netzsch LFA 457. The geometrical density of the bars was determined from their dimensions and the mass and the heat capacity was estimated by the Dulong-Petit law. Furthermore, we tested the mechanical properties by Vickers hardness measurements with a Struers Dura-Scan-20, applying a force of 0.3 kgfs on the polished and coplanar samples. The uncertainties were 3% for the electrical conductivity and thermal diffusivity, and 5% for the Seebeck coefficient, leading to an 11% uncertainty in the *ZT* values. We repeated the experiments numerous times and have confirmed that the peak *ZT* values were reproducible within 5%. Furthermore, we measured the samples while heating up to 700°C and cooling and found that there was no degradation in the individual properties.

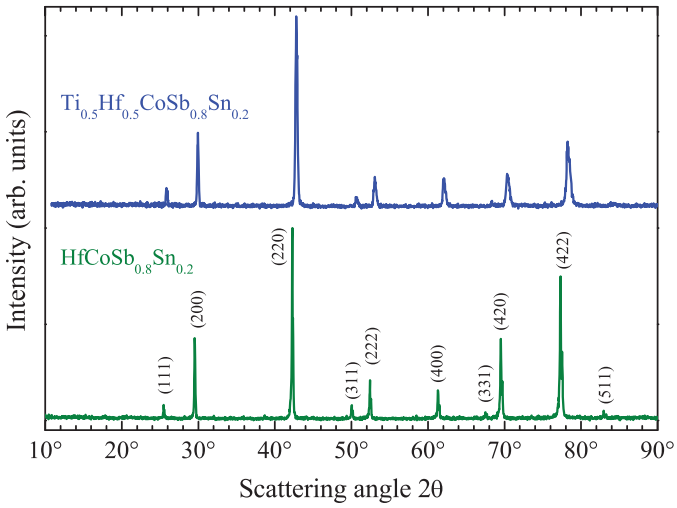

Fig. 1 Representative X-ray powder diffraction patterns of samples with $M = Ti_{0.5}Hf_{0.5}$ and *M* = Hf.

3 Results and discussion

3.1 Structural investigations

The $C1_b$ structure of all samples was confirmed by PXRD analysis of the powder samples. All samples were phase-pure despite a marginal amount of β-Sn (1.2%), which is close to the detection limit. Representative PXRD measurements of $HfCoSb_{0.8}Sn_{0.2}$ and $Ti_{0.5}Hf_{0.5}CoSb_{0.8}Sn_{0.2}$ are shown in Fig. 1. The position of the main (220) reflection of $Ti_{0.5}Hf_{0.5}CoSb_{0.8}Sn_{0.2}$ is shifted to a higher scattering angle due to the decrease of the lattice parameter upon substitution of Hf by Ti, as one would expect on the basis of the atomic radii of the elements. The reflections at higher scattering angles ((400), (420), and (422)) are sharper for $HfCoSb_{0.8}Sn_{0.2}$, whereas in the case of $Ti_{0.5}Hf_{0.5}CoSb_{0.8}Sn_{0.2}$ the peaks are broader and asymmetric.

Table 1 Composition and phases of the samples MCoSb$_{0.8}$Sn$_{0.2}$ as determined by EDX spectroscopy, and experimental density ρ and Vickers hardness HV0.3.

M	Composition	Phases	ρ/ g/cm^3	HV0.3
Ti	$Ti_{0.97}Co_{0.99}Sb_{0.79}Sn_{0.25}$	$Ti_{1.01}Co_{0.97}Sb_{0.91}Sn_{0.1}$ $Ti_{0.91}Co_{1.19}Sb_{0.23}Sn_{0.67}$	7.21	783
Zr	$Zr_{1.01}Co_{0.96}Sb_{0.77}Sn_{0.25}$	$Zr_{1.02}Co_{0.96}Sb_{0.87}Sn_{0.16}$ $Zr_{1.01}Co_{0.96}Sb_{0.15}Sn_{0.88}$	7.69	810
Hf	$Hf_{1.07}Co_{0.93}Sb_{0.80}Sn_{0.20}$	$Hf_{1.11}Co_{0.92}Sb_{0.83}Sn_{0.14}$ $Hf_{0.89}Co_{1.28}Sb_{0.07}Sn_{0.76}$	10.17	882
$Ti_{0.5}Zr_{0.5}$	$Ti_{0.49}Zr_{0.50}Co_{0.94}Sb_{0.89}Sn_{0.18}$	$Ti_{0.45}Zr_{0.56}Co_{0.96}Sb_{0.94}Sn_{0.09}$ $Ti_{0.64}Zr_{0.38}Co_{0.98}Sb_{0.89}Sn_{0.13}$	7.43	716
$Zr_{0.5}Hf_{0.5}$	$Zr_{0.47}Hf_{0.56}Co_{0.94}Sb_{0.84}Sn_{0.19}$	$Zr_{0.47}Hf_{0.56}Co_{0.93}Sb_{0.88}Sn_{0.15}$ $Zr_{0.52}Hf_{0.51}Co_{0.97}Sb_{0.72}Sn_{0.28}$	9.22	846
$Ti_{0.5}Hf_{0.5}$	$Ti_{0.52}Hf_{0.56}Co_{0.98}Sb_{0.65}Sn_{0.29}$	(I) $Ti_{0.65}Hf_{0.31}Co_{1.21}Sb_{0.23}Sn_{0.61}$ (II) $Ti_{0.38}Hf_{0.70}Co_{0.98}Sb_{0.84}Sn_{0.1}$	9.38	868

This is a strong indication of the existence of a second phase with a slightly different lattice parameter (see Fig. 2 for the EDX results). Investigation of the analogous *n*-type Heusler compound $Ti_{0.5}Zr_{0.25}5Hf_{0.25}NiSn$ by synchrotron radiation revealed a splitting of the main reflex (220) into a triple peak corresponding to three Heusler phases.[22] Therefore, it is reasonable that the same effect could occur in the *p*-type system.

As shown in Table 1, the overall composition of all samples as analyzed by EDX spectroscopy agrees well with their nominal composition, which indicates that no significant loss of Sb took place. Samples without substitution at the M position (M = Ti, Zr or Hf) show a homogeneous distribution of all elements apart from some minor variations of the Sn and Sb content. Further, the alloying of Zr and Hf did not result in phase separation because the chemical behavior of both atoms is very similar and they have nearly the same atomic radii caused by the Lanthanide contraction. This confirms the results previously reported by Culp et al.[11] The secondary electron (SE) image of $Zr_{0.5}Hf_{0.5}CoSb_{0.8}Sn_{0.2}$ (see Fig. 2a) shows the typical microstructure of the samples with M = Ti, Zr, Hf or $Zr_{0.5}Hf_{0.5}$. The matrix with composition $Zr_{0.45}Hf_{0.55}Co_{0.95}Sb_{0.9}Sn_{0.1}$ is interspersed with some darker regions of $Zr_{0.5}Hf_{0.5}CoSb_{0.7}Sn_{0.3}$. Additionally, some very bright spots, which can be identified as Sn inclusions, are visible.

Contrarily, the mixing of Ti with Zr results in areas with slightly more Ti ($Ti_{0.4}Zr_{0.6}$) or slightly more Zr ($Ti_{0.6}Zr_{0.4}$). Still the composition changes continuously and no clear phase boundaries are observed. This effect is even more enhanced when Ti is alloyed with Hf. The secondary electron image of $Ti_{0.5}Hf_{0.5}CoSb_{0.8}Sn_{0.2}$ in Fig. 2b shows separation into a two-phase microstructure: a dendritic structure consisting of a Hf- and Sb-rich Heusler phase (phase II), with an approximate composition of $Ti_{0.4}Hf_{0.7}CoSb_{0.85}Sn_{0.1}$, in a Ti- and Sn-rich matrix $Ti_{0.65}Hf_{0.3}Co_{1.2}Sb_{0.2}Sn_{0.6}$ (phase I). The bright spots are again identified as Sn inclusions, whereas the black spots are Hf.

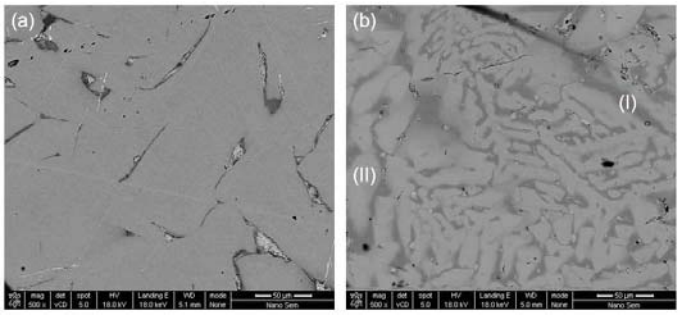

Fig. 2 Secondary electron image of $Zr_{0.5}Hf_{0.5}CoSb_{0.8}Sn_{0.2}$ (a) in comparison to $Ti_{0.5}Hf_{0.5}CoSb_{0.8}Sn_{0.2}$ (b).

Since the mechanical stability of a TE material is very important for application and processing, the Vickers hardnesses of the compounds were investigated at room temperature. The values are presented in Table 1. All compounds show relatively high intrinsic hardness, which corresponds to the previously reported values for the *n*-type material based on MNiSn.[23] This is favorable for the co-processing of the *n*- and *p*-type materials in a TE device.

3.2 Thermoelectric properties

The temperature dependence of the thermal conductivity κ, electrical conductivity σ, and Seebeck coefficients S of MCoSb$_{0.8}$Sn$_{0.2}$ (M = Ti, Zr, Hf, $Ti_{0.5}Zr_{0.5}$, $Zr_{0.5}Hf_{0.5}$, and $Ti_{0.5}Hf_{0.5}$) are plotted in Fig. 3. The thermal conductivity of nonsubstituted compounds (M= Ti, Zr, or Hf) decreased with increasing temperature and exhibited the highest values. The values of κ decreased for solid-solution alloying of

M = $Ti_{0.5}Zr_{0.5}$ and $Zr_{0.5}Hf_{0.5}$ due to the mass differences of Ti, Zr, and Hf atoms. This reduced the lattice thermal conductivity through chemical disorder scattering. The nearly constant value of κ for the composition $Ti_{0.5}Hf_{0.5}$ over the whole temperature range is remarkable indicating a glass-like behaviour. With a value of 3.2 W/(m*K) a reduction of 39% compared to $TiCoSb_{0.8}Sn_{0.2}$ at 700 °C was achieved. In this case, the presence of the intrinsic microstructure leads to additional boundary scattering at the interfaces and hence to a reduction of the lattice thermal conductivity. Comparable small values reported in the literature were only achieved by micro- or nano-structuring using a ball-milling process[4,5,7] or by the embedding of nanoinclusions.[24,25] For comparison, the transport properties of nanostructured compounds made by Yan et al.[5] with the composition $Ti_{0.5}Hf_{0.5}CoSb_{0.8}Sn_{0.2}$ are plotted.

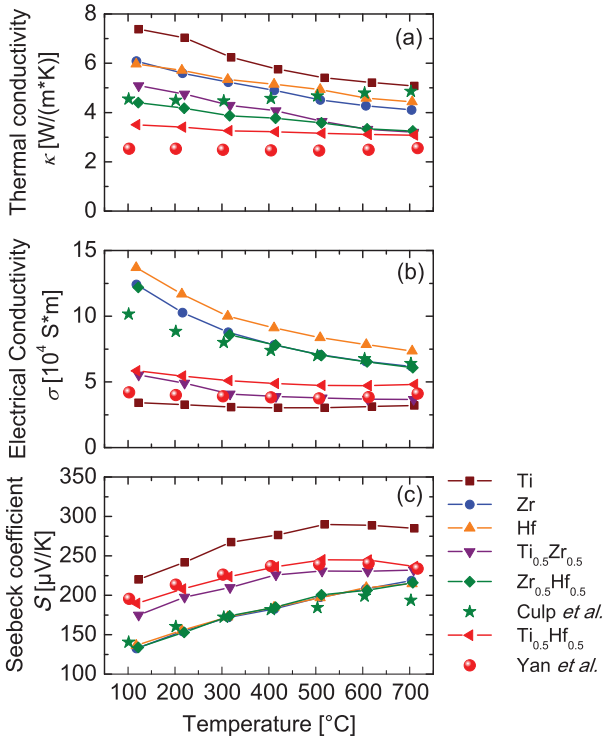

Fig. 3 (a) Thermal conductivity κ, (b) electrical conductivity σ, and (c) Seebeck coefficient S as a function of temperature for $M$$CoSb_{0.8}Sn_{0.2}$ with the indicated composition of M. Comparison with values reported in the literature for M = $Zr_{0.5}Hf_{0.5}$ ($\star$ ingot sample)[11] and M = $Ti_{0.5}Hf_{0.5}$ (● nanostructured sample).[5]

All samples show metallic behavior as the electrical conductivity σ decreases with increasing temperature (Fig. 3b). The composition $TiCoSb_{0.8}Sn_{0.2}$ exhibited the lowest value of σ. The values increased upon substitution of Ti with the heavier homologous Zr and Hf, indicating an increase in the charge carrier concentration.

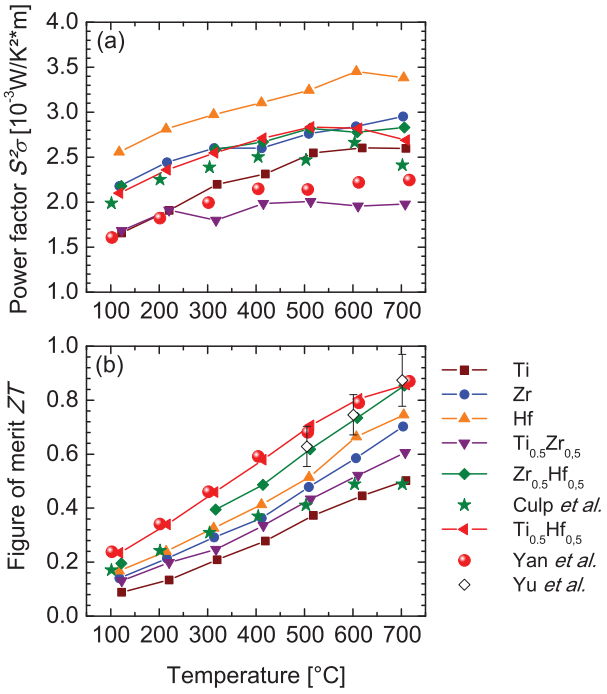

Fig. 4 (a) Power factor PF and (b) Figure of merit ZT as a function of temperature for $M$$CoSb_{0.8}Sn_{0.2}$ with the indicated composition of M. Comparison with values reported in the literature for M = $Zr_{0.5}Hf_{0.5}$ ($\star$ ingot sample),[11] M = $Ti_{0.5}Hf_{0.5}$ (● nanostructured sample),[5] and the best SiGe-based p-type material $(Si_{95}Ge_5)_{0.65}(Si_{70}Ge_{30}P_3)_{0.35}$ (◇).[2]

All measured Seebeck coefficients are positive, indicating p-type transport behavior. The temperature dependency shows an almost linear increase. The maximum was not reached in the experimental temperature range, which is very attractive for high-temperature applications. Contrary to the electrical conductivity, the highest Seebeck coefficient of 289.9 μV/K (at 600 °C) was obtained for $TiCoSb_{0.8}Sn_{0.2}$. Alloying of Zr and Hf does not effect the Seebeck coefficient significantly. The corresponding values of S for M = Zr, Hf, and $Zr_{0.5}Hf_{0.5}$ are similar. In contrast, the alloying of Zr and Hf by Ti enhances the Seebeck coefficient and reaches a value of 244.7 μV/K at 600 °C for M = $Ti_{0.5}Hf_{0.5}$, whereas the unsubstituted $ZrCoSb_{0.8}Sn_{0.2}$ and $HfCoSb_{0.8}Sn_{0.2}$ only achieve a value of 208.1 μV/K and 209.8 μV/K respectively.

The calculation of the power factor $S^2\sigma$ reveals that both effects nearly compensate for each other. As shown in Fig. 4a, the absolute values are between 1.94 mW/(K^2m) for $Ti_{0.5}Zr_{0.5}$ and 3.38 mW/(K^2m) at 700 °C for Hf.

By combining the electronic properties with the previously discussed thermal conductivity, we obtained a maximal ZT of approximately 0.9 at 700°C for $Ti_{0.5}Hf_{0.5}$ and $Zr_{0.5}Hf_{0.5}$. Comparable high ZT values for p-type Heusler systems have

only been reported for a nanostructure approach via ball milling.[4,5] More promising is that the value of the Heusler compound obtained in the current study is comparable with the record *p*-type value based on SiGe alloying, as shown in Fig. 4b.[2] Here it is important to keep in mind that the basic cost of the Heusler TE is approximately 60% lower than that of SiGe.[26]

4 Conclusions

An intrinsic phase separation in the *p*-type Heusler system (Ti/Zr/Hf)$CoSb_{0.8}Sn_{0.2}$ was obtained by applying isoelectronic alloying analogous to the *n*-type system.[22] Mandatory was the partial substitution of Ti with Hf, which resulted in nanostructuring of the system consisting of at least two stable Heusler phases – one rich in Ti and Sn and the other rich in Hf and Sb. Similar to the TiNiSn system a dendritical phase separation was observed. Subsequently, the thermal conductivity was reduced to 3.2 W/(m*K) in $Ti_{0.5}Hf_{0.5}CoSb_{0.8}Sn_{0.2}$, which is an improvement of approximately 40% as compared to $TiCoSb_{0.8}Sn_{0.2}$. This led to a maximum *ZT* of 0.9 at 700 °C, i.e. a 80% enhancement in peak *ZT* from 0.5 to 0.9 compared to the best published value of an ingot *p*-type Half-Heusler compound.[4] The high hardness and the similarity of the values to those of the *n*-type material is an advantage for the construction of TE modules based on Heusler compounds. This initial proof-of-concept can serve as a very useful starting point for the design of new materials for high-temperature thermoelectric applications.

5 Acknowledgements

The authors gratefully acknowledge the financial support by the German Research Foundation (DFG Priority Program 1386 ”Nanostructured Thermoelectric Materials” under proposal BA 4171/2-2) and the thermoHeusler Project (Project No. 0327876D) of the German Federal Ministry of Economics and Technology (BMWi).

References

1 S. A. Yamini, H. Wang, Z. M. Gibbs, Y. Pei, S. X. Doua and G. J. Snyder, *Phys.Chem.Chem.Phys.*, 2014, **16**, 1835.
2 B. Yu, M. Zebarjadi, H. Wang, K. Lukas, H. Wang, D. Wang, C. Opeil, M. Dresselhaus, G. Chen and Z. Ren, *Nano Lett.*, 2012, **12**, 2077.
3 M. Schwall and B. Balke, *Appl. Phys. Lett.*, 2011, **98**, 042106.
4 X. Yan, G. Joshi, W. Liu, Y. Lan, H. Wang, S. Lee, J. W. Simonson, S. J. Poon, T. M. Tritt, G. Chen and Z. F. Ren, *Nano Lett.*, 2011, **11**, 556–560.
5 X. Yan, W. Liu, H. Wang, S. Chen, J. Shiomi, K. Esfarjani, H. Wang, D. Wang, G. Chen and Z. Ren, *Energy Environ. Sci.*, 2012, **5**, 7543.
6 K. Bartholome, B. Balke, D. Zuckermann, M. Köhne, M. Müller, K. Tarantik and J. König, *J. Electron. Mater.*, 2013, 1–7.
7 P. Maji, J. P. A. Makongo, X. Zhou, H. Chi, C. Uher and P. F. P. Poudeu, *J. Solid State Chem.*, 2013, **202**, 70–76.
8 T. Graf, C. Felser and S. S. P. Parkin, *Progress in Solid State Chemistry*, 2011, **39**, 1–50.
9 S. Ouardi, G. H. Fecher, C. Felser, M. Schwall, S. S. Naghavi, A. Gloskovskii, B. Balke, J. Hamrle, K. Postava, J. Pištora, S. Ueda and K. Kobayashi, *Phys. Rev. B*, 2012, **86**, 045116.
10 S. Chen and Z. Ren, *Materials Today*, 2013, **16**, 387.
11 S. R. Culp, J. W. Simonson, S. J. Poon, V. Ponnambalam, J. Edwards and T. M. Tritt, *Appl. Phys. Lett.*, 2008, **93**, 022105.
12 C.-C. Hsu, Y.-N. Liu and H.-K. Ma, *J. Alloys Compd.*, 2014, **597**, 217–222.
13 L.-D. Zhao, V. P. Dravid and M. G. Kanatzidis, *Energy Environ. Sci.*, 2014, **7**, 251–268.
14 M. G. Kanatzidis, *Chemistry of Materials*, 2009, **22**, 648–659.
15 Y. Gelbstein, J. Davidow, S. N. Girard, D. Y. Chung and M. Kanatzidis, *Adv. Energy Mater.*, 2013, **3**, 815–820.
16 K. Kurosaki, T. Maekawa, H. Muta and S. Yamanaka, *Journal of Alloys and Compounds*, 2005, **397**, 296–299.
17 Y. Kimura, H. Ueno and Y. Mishima, *Journal of Electronic Materials*, 2009, **38**, 934–939.
18 S. Populoh, M. H. Aguirre, O. C. Brunko, K. Galazka, Y. Lu and A. Weidenkaff, *Scripta Materialia*, 2012, **66**, 1073–1076.
19 T. Graf, P. Klaer, J. Barth, B. Balke, H.-J. Elmers and C. Felser, *Scripta Materialia*, 2010, **63**, 1216–1219.
20 N. Shutoh and S. Sakurada, *J. Alloys Compd.*, 2005, **389**, 204–208.
21 S. Sakurada and N. Shutoh, *Appl. Phys. Lett.*, 2005, **86**, 082105.
22 M. Schwall and B. Balke, *Phys.Chem. Chem. Phys.*, 2013, **15**, 1868.
23 M. A. Verges, P. J. Schilling, P. Upadhyay, W. K. Miller, R. Yaqub, K. L. Stokes and P. F. P. Poudeu, *Sci. Adv. Mater.*, 2011, **3**, 659666.
24 P. Sahoo, Y. Liu, J. P. A. Makongo, X.-L. Su, S. J. Kim, N. Takas, H. Chi, C. Uher, X. Pan and P. F. P. Poudeu, *Nanoscale*, 2013, **5**, 9419.
25 T. Wu, W. Jiang, X. Li, Y. Zhou and L. Chen, *J. Appl. Phys.*, 2007, **102**, 103705.
26 S. LeBlanc, S. K. Yee, M. L. Scullin, C. Dames and K. E. Goodson, *Renew. Sust. Energ. Rev.*, 2014, **32**, 313–327.